Available online at www.sciencedirect.com
ScienceDirect
Journal of the European Ceramic Society 29 (2009) 293–303
www.elsevier.com/locate/jeurceramsoc

Light scattering in polycrystalline alumina with bi-dimensionally large surface grains

H.N. Yoshimura [a,*], H. Goldenstein [b]

[a] Institute for Technological Research of the State of São Paulo, Av. Prof. Almeida Prado, 532 São Paulo, SP, 05508-901, Brazil
[b] Polytechnic School of the University of São Paulo, Av. Prof. Mello Moraes, 2463 São Paulo, SP, 05508-900, Brazil

Available online 1 May 2008

Abstract

Alumina ceramics with high in-line transmittance at 0.5–1.0 mm-thickness were prepared with different doping additives by sintering at 1850 °C in vacuum for 1–8 h. Depending on the additive contents and sintering variables bi-dimensionally large surface grains, caused by surface evaporation of MgO, had grown parallel to the surface with ~100 μm thickness and lateral sizes up to the millimeter range. The abnormal grain-growth process also resulted in the formation of pores entrapped inside the large surface grains within a narrow zone at 10–20 μm distance from the surface. The fraction of these pores is thickness-invariant. Scattering factors associated to the pores entrapped inside the bi-dimensionally large surface grains, second-phase particles, grain-boundaries, and microstructural surface defects are derived from the results of in-line transmission (at 600 nm) and are used together with microstructural characteristics to explain the light transmittance in these materials.

Keywords: Alumina; Microstructure; Optical property; Scattering; Sintering

1. Introduction

Translucent polycrystalline alumina (TPCA) has been used as electric arc discharge envelops for high intensity discharge (HID) lamps, windows for erasable programmable read-only memories (EPROMs), dental brackets, and components for chemical plants. High optical transmittance, corrosion resistance, refractoriness, and good mechanical properties are some characteristics of this ceramic. The key factor to produce TPCA is the control of microstructure evolution during sintering, in order to result in an almost single-phase, fully dense polycrystalline ceramic body. The starting powder characteristics determine the sintering behavior and optical properties; therefore high-purity alumina powders with high sinterability have been used. A small amount of MgO (~500 ppm or higher) as grain-growth inhibitor, a gas soluble in alumina (usually hydrogen) or vacuum as sintering atmosphere, and a high sintering temperature (~1800–1900 °C) have been used to guarantee the elimination of most of the residual pores during the sintering.[1,2]

Light scattering by residual sintering pores strongly affects the light transmission of TPCA, because of the significant difference between the refractive index of alumina and vacuum. Mie scattering model explains the pore size dependence and predicts that the maximum scattering occurs when the pores are almost as large as the wavelength of the incident light.[3,4] Scattering and absorption from residual second-phase particles, like spinel ($MgAl_2O_4$), also affect light transmission. TPCA presents high total transmittance (direct and diffuse transmitted light), but low in-line transmittance (direct transmitted light), because of the forward scattering caused by pores, second-phases, and grain-boundaries (related to the birefringence of alumina). Others factors that affect the light transmission are reflectance at the TPCA surfaces and surface roughness (like thermal grooves of grain-boundaries on the surface of as-sintered products).[4]

The in-line transmittance, T_I, of TPCA can be expressed by Beer–Lambert–Budworth equation:[5]

$$T_I = (1 - R)^2 \exp[-(\alpha + S_p + S_b)t] \quad (1)$$

where R is the reflectance; α is the intrinsic absorption coefficient; S_p is the scattering coefficient related to the second-phase particles, including pores; S_b is the scattering coefficient related to grain-boundaries; t is the thickness. It has been demonstrated that in-line transmittance of TPCAs with polished surfaces follows this equation and the in-line loss coefficient

* Corresponding author. Tel.: +55 11 3767 4057; fax: +55 11 3767 4037.
E-mail address: hnyoshim@ipt.br (H.N. Yoshimura).

0955-2219/$ – see front matter © 2008 Elsevier Ltd. All rights reserved.
doi:10.1016/j.jeurceramsoc.2008.03.008

$(\alpha + S_p + S_b)$ has been determined. In the visible region, high values have been reported: 3.8 and 4.9 mm^{-1} at wavelength of 500 nm for hot-pressed and sintered alumina, respectively;[3] and 1.06 and 0.87 mm^{-1} at 700 nm for sintered alumina with different additive systems (MgO–CaO and MgO–Y_2O_3–CaO, respectively).[6] Significantly lower values have been reported in the infrared region: 0.30 mm^{-1} at 4.5 μm for sintered alumina;[7] and 0.15 mm^{-1} at 4.5 μm for hot-forged alumina.[8]

The low in-line transmittance limits the use of TPCA for products that do not need image definition of an object posted at some distance behind them. The development of TPCA with higher in-line transmittance is desirable, for example for the improvement of aesthetic quality of dental brackets. There are some additive systems proposed to improve light transmittance of TPCA, but all have MgO as main component, as first proposed by Coble,[1] like MgO–Y_2O_3,[9] MgO–Y_2O_3–La_2O_3,[10,11] MgO–ZrO_2/HfO_2,[12] and MgO–ZrO_2–CaO systems.[13] Co-doping with Y_2O_3 seems to increase the densification rate of alumina[9] and the co-doping with ZrO_2 and/or HfO_2 seems to increase the solubility of MgO, lowering the evaporation of MgO from the surface.[12] During the sintering, MgO evaporates from the surface of alumina body, causing the occurrence of abnormal grain growth (AGG). As a consequence, a higher amount of MgO in starting powder is used to assure that the MgO content in the depleted MgO layer do not lower bellow a critical level (~60 ppm), at which AGG starts to occur.[14,15] This procedure results in a fraction of spinel particles, which scatter the light. When low MgO content is used, very large grains (2–10 mm in size) are formed on the surfaces, with thickness relatively small and constant (~10–40 μm).[16] Based on the evaporation of MgO at high temperature and the occurrence of AGG, a solid-state conversion method of TPCA to a single-crystal alumina body was proposed.[17,18] The AGG can be induced by a localized SiO_2 co-doping, resulting in the conversion of surface regions to single-crystal sapphire layers (thickness ranging from ~100 to 200 μm) with a polycrystalline core; such material presented a high value of in-line transmittance (35%), nearly four times that of unconverted TPCA and approaching that of melt-grown sapphire (50%).[19] Recently, it has been demonstrated that alumina with submicrometer grain size and very high in-line transmittance in the visible region can be prepared by hot isostatic pressing (HIPing).[20,21] The scattering mechanism changes in submicrometer grain size range and a Rayleigh–Gans–Debye light-scattering theory has been applied to explain the light transmittance of this new material.[4]

In this work, the optical transmittance of vacuum sintered TPCA with bi-dimensionally large surface (BLS) grains are investigated. The aim of this work was to develop a TPCA with BLS grains with high transparency and to understand its optical behavior. TPCA with high in-line transmittance in the visible region could be prepared using MgO–CaO and MgO–Y_2O_3–CaO additive systems. Based on in-line transmittance measurement and microstructure analysis, an additional scattering factor to Beer–Lambert–Budworth equation was proposed. The scattering coefficients were evaluated and the effects of each optical inhomogeneity could be determined.

2. Experimental

A high-purity alumina powder (Showa Denko, UA-5105, 0.6 μm, 9 m^2/g), reagent grade magnesium nitrate ($Mg(NO_3)_2 \cdot 6H_2O$, Merck), yttrium nitrate ($Y(NO_3)_3 \cdot 6H_2O$, Merck), and calcium chloride ($CaCl_2 \cdot 2H_2O$, Mallinckrodt), and 2% polyvinyl alcohol and 0.5% polyethylene glycol, as binders, were wet mixed for 6 h using distilled and demineralized water. The salt contents were adjusted to prepare three samples with different additive systems:

(i) sample M: 300 ppm MgO;
(ii) sample MC: 300 ppm MgO +150 ppm CaO;
(iii) sample MYC: 300 ppm MgO +100 ppm Y_2O_3 +50 ppm CaO.

After drying, the powder was granulated using a 35-mesh nylon screen, in order to avoid contamination from metal screen. The granules were uniaxially pressed at 200 MPa in a tungsten carbide die to form disc-shaped green bodies with diameter of 15 mm and thickness adjusted to result in sintered bodies with thickness of ~0.5, 0.7 and 1.0 mm. All powder-processing stages were conducted in a clean room class 10^5, in order to minimize powder contamination, such as SiO_2 impurity. The green bodies were pre-sintered in air at 1100 °C for 1 h after a debinding step at 300 °C for 2 h. Calcined bodies were sintered in a tungsten heated furnace (NM-15, Nems), inside a molybdenum crucible, at 1850 °C for 1, 3, 5 and 8 h under vacuum (~10^{-3} Pa); the heating and cooling rates were 15 and 60 °C/min, respectively. Five specimens were prepared for each investigated condition.

Chemical analysis of granulated powders and sintered samples was conducted in an inductively coupled plasma (ICP) spectrometer (SPS 1700R, Seiko) in order to quantify the additive loss during sintering. In-line transmittance of as-sintered specimens (without surface polishing) was measured in a spectrophotometer (U-3000, Hitachi) with a slit of 0.2 nm at wavelength of 600 nm. Microstructural analysis was performed in an optical microscope (OM, Zeiss). For the direct analysis of internal microstructure, the specimen was immersed in CH_2I_2 liquid, which refractive index of 1.74 is close to the alumina (1.76), to facilitate the observation of light scattering centers inside the material using the OM with transmitted light.[22] The cross-section microstructures of the samples were analyzed after cutting the specimen near the center, polishing the transverse surface, and thermal etching the polished surface to reveal the grain-boundaries. Grain size of internal polycrystalline region was determined by planimetric method (ASTM E 112—Standard test methods for determining average grain size). The average grain size, G, was calculated as mean lineal intercept, as has been suggested for the analysis of grain-boundary scattering coefficient.[5,23] The thickness of the bi-dimensionally large surface grains was measured on polished and etched cross-section using a graduated scale attached to the OM, operating with reflected light.

3. Results

3.1. Microstructure

Huge grains, with lateral sizes from ~0.5 to 5 mm, were observed on the surfaces of the three samples (M, MC and MYC) sintered at 1850 °C for 1–8 h (Fig. 1a and b). Regions of residual small grains enclosed among huge grains were occasionally observed (Fig. 1c). The sample MYC sometimes presented, instead of huge grains (b), smaller grains on the surface (d); these grains, however, were larger than the grains of internal region of the sintered body (Fig. 2c). The huge grains were flat, with thickness of ~100 μm and almost constant throughout the specimen (Fig. 2). The microstructure looked like as a translucent polycrystalline alumina with a layer of alumina single-crystal platelets bonded on the surface. Based on this association, the microstructure, hereinafter, is described as an internal polycrystalline region covered by bi-dimensionally large surface (BLS) grains. The formation of BLS grains in the samples M, MC and MYC is in accordance to the results observed before that these grains form suddenly above ~1800 °C in alumina doped with MgO content bellow ~600 ppm.[24]

The thickness of BLS grains and the grain size of internal polycrystalline region were not significantly affected by the thickness of the sample. They were, however, influenced by sintering time and additive composition (Fig. 3). The grain growth in internal polycrystalline region close followed the cubic law, as has been observed for high-purity alumina doped with MgO,[25] but the thickness of BLS grains increased at slower rates. The grain size of sample M varied between 13 and 25 μm, when sintered between 1 and 8 h and was slight smaller than the samples MC and MYC, which achieved a grain size of ~30 μm after sintering for 8 h. In the case of thickness of BLS grains, the sample MYC presented higher values (~90–130 μm, when sintered between 1 and 8 h) than the samples M and MC, which maximum thickness was ~110 μm (Fig. 3).

The light scattering centers inside the samples could be directly observed using the transmission optical microscope with the specimens immersed in liquid CH_2I_2. Changing the focus inside the material, a thin layer of pores could be observed inside the BLS grains (Fig. 4). The maximum fraction of pores was observed at a distance of ~10–20 μm from the surface. The remaining thickness of BLS grains was free of pores and second-phases. The fraction of pores entrapped inside BLS grains varied strongly among the three samples. Sample M presented the highest fraction of pores (Fig. 4a), followed by the sample MC (b), while sample MYC presented very low fraction of pores (c). The layer of pores entrapped inside BLS grains was parallel to the surface and the fraction of pores was almost constant throughout the sample. In the regions around the grain-boundaries, smaller amounts of pores were observed. This result indicated that diffusion of vacancies through the grain-boundaries and free surface eliminated some pores entrapped inside BLS grains. It was not observed, however, significant variation of the fraction of these pores among samples sintered at different times (1–8 h).

In the internal polycrystalline region, sample MC presented a dispersion of second-phase particles with size of ~1 μm (Fig. 5a). The contrast between particles and alumina matrix was slightly higher than that observed between alumina and spinel (refractive index of 1.72),[26] because of the presence of CaO in this sample. No significant difference related to the second-phase particles could be observed among the specimens sintered at different temperatures and with different thickness, even though a slight particle coarsening was observed with the increase of sintering time in this sample (MC). Sample MYC presented a small fraction of second-phase particles (~1 μm) after sintering for 1 h (Fig. 5b). The volume fraction and the size of particles in this sample increased with the increase of sintering time and some particles with sizes of up to ~5 μm were observed in the specimens sintered for 8 h (c). The second-phase particles in the sample MYC were darker than those observed in sample MC. A previous study of transmission electron microscopy and energy dispersive spectroscopy in a similar sample (alumina doped with 300 ppm MgO, 100 ppm Y_2O_3 and 150 ppm CaO) showed that the second-phase particles were an aluminum, yttrium oxide, possibly YAG ($Y_3Al_5O_{12}$).[24] This oxide has a high refraction index (1.84),[26] which seems to justify the darker particles observed in the sample MYC (Fig. 5c). The analysis of internal polycrystalline region of the sample M was difficult to be conducted, because of the significant light scattering caused by the pores entrapped inside BLS grains (Fig. 4a). The analysis, however, indicated that the sample M was almost free of spinel particles. All three samples almost did not present residual pores in the internal polycrystalline region (Fig. 5).

The results of chemical analysis of the sample before and after the sintering are shown in Table 1. All three samples presented a reduction of the MgO content during the sintering, but the reduction varied among the samples: 27, 47 and 81% for samples M, MC and MYC, respectively. These results showed that the addition of CaO and Y_2O_3 increased the evaporation rate of MgO. CaO content of the samples MC and MYC was also significantly reduced (61 and >91%, respectively). Y_2O_3 content in sample MYC, however, almost did not vary during the sintering. The results of chemical analysis were in accordance to the microstructure characteristics observed in the internal polycrystalline region (Fig. 5). The solubility limit of MgO in alumina is ~150 ppm at 1850 °C.[15] Since MgO content above this limit in sample M was ~80 ppm, the expected volume fraction of spinel ($MgAl_2O_4$) is very low (~0.03 vol.%), as was anticipated by microstructural analysis. This result is in accordance to that reported by Apetz and Van Bruggen[4] which observed no significant effect of MgO on the optical properties of TPCA up to a MgO content of 300 ppm. Sample MC presented 158 ppm of MgO and 62 ppm of CaO after sintering (Table 1). The possible intermediate phase in the system Al_2O_3–CaO–MgO is $Ca_3MgAl_4O_{10}$,[27] which seems to have slight higher refractive index than spinel, as mentioned before (Fig. 5a). Sample MYC presented after sintering 58 ppm of MgO, 95 ppm of Y_2O_3, and almost zero of CaO (Table 1). This result reinforces that the dark second-phase particles in this sample (Fig. 5c) were YAG phase. This phase was also observed in TPCA prepared with 500 ppm MgO and 350 ppm Y_2O_3.[14]

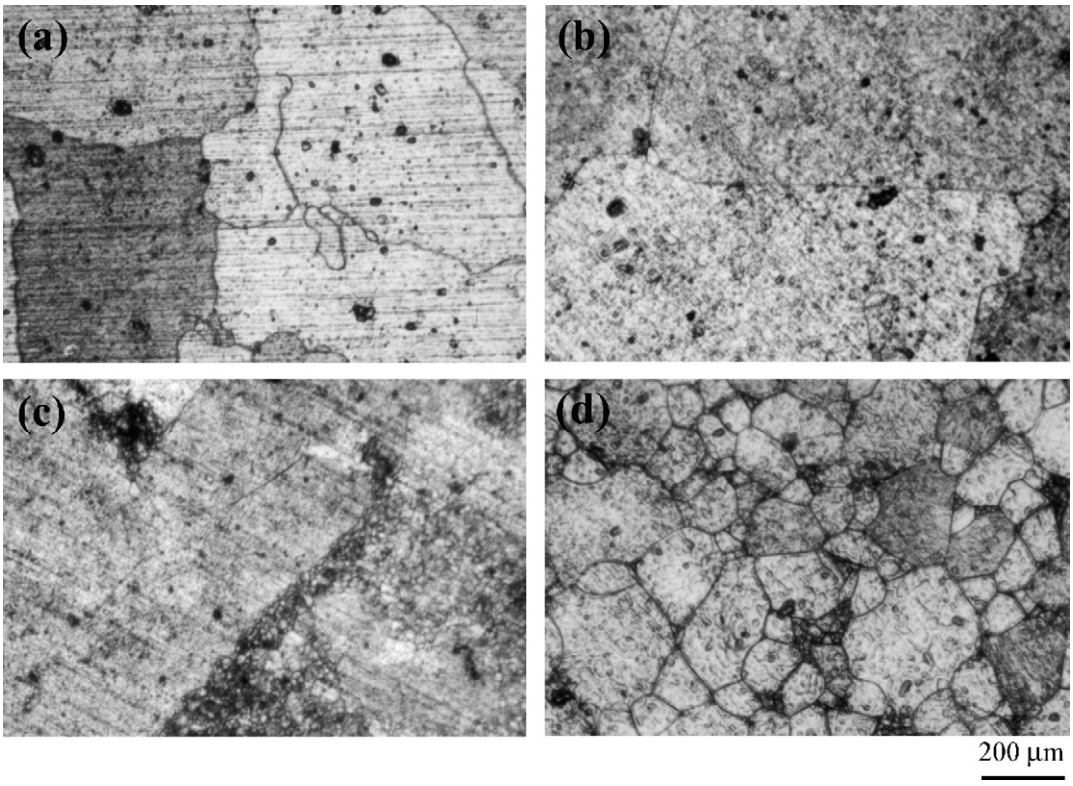

Fig. 1. OM images (reflected light) of the as-sintered surface of: (a) sample M sintered for 8 h; (b) sample MYC sintered for 3 h; (c) sample MC sintered for 3 h; (d) sample MYC sintered for 8 h.

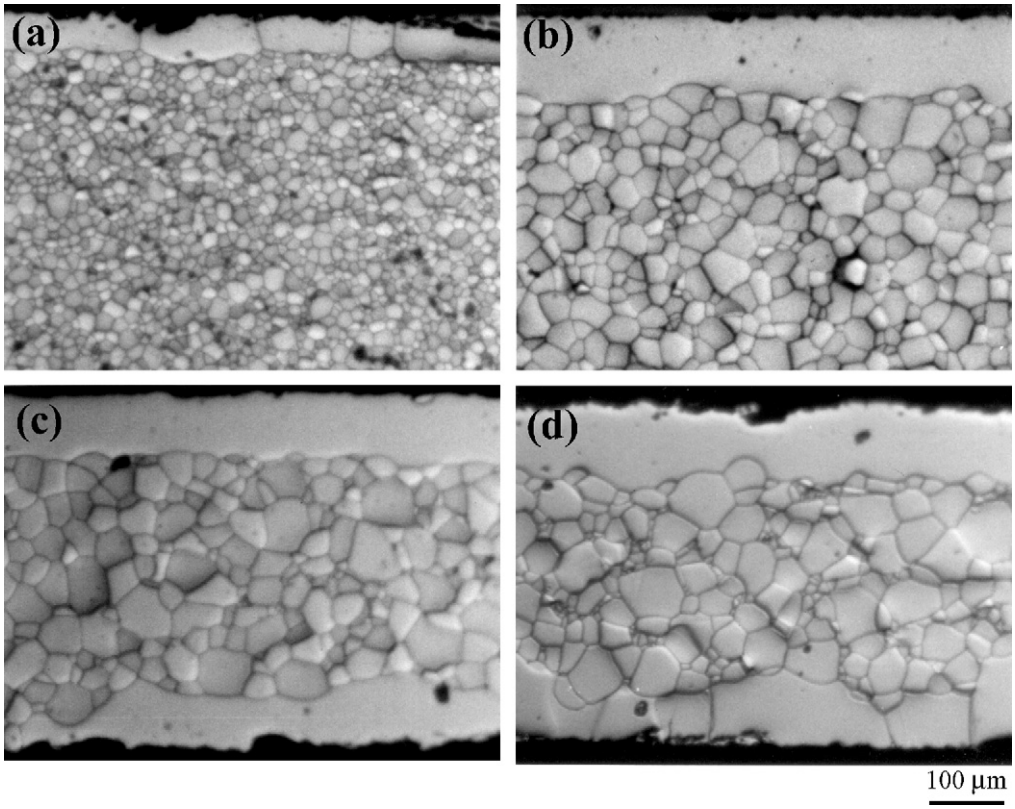

Fig. 2. OM images (reflected light) of the cross-section of: (a) sample M (thickness of 1 mm) sintered for 1 h; (b) sample M (0.7 mm) sintered for 8 h; (c) sample MC (0.5 mm) sintered for 3 h; (d) sample MYC (0.5 mm) sintered for 3 h. The dark regions are grain pullouts or border scratching which occurred during the sample preparation.

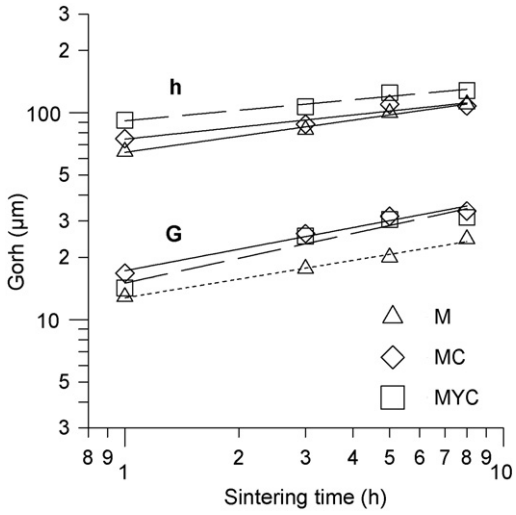

Fig. 3. Grain size (G) of internal polycrystalline region and thickness of BLS grains (h) as a function of sintering time (1850 °C).

3.2. Light transmission

Sample MYC (300 MgO–150 Y_2O_3–50 CaO, in ppm) presented significantly higher in-line transmittance; the highest value measured was 43.4% at 0.5 mm thickness (Fig. 6a). Sample M (300 ppm MgO) presented the lowest transmittance, with values almost half of the sample MYC (Fig. 6b). The in-line transmittance increased logarithmically with the increase of sintering time and, for each sample, the angular coefficient of these fits did not vary significantly among the specimens with different thickness (a). The transmittance of sample MYC increased at an average rate almost two times of those observed in samples M and MC (b).

The in-line transmittance of the three samples decreased exponentially with the increase of thickness (Fig. 7), as predicted by Eq. (1). Considering the reflectance, R, of alumina single-crystal (0.074), the predicted light transmission loss by reflection at both surfaces is 14.3%.[6] Therefore, for a TPCA with homogeneous distribution of scattering centers throughout the volume, the transmittance should converge to the value of 85.7% at zero thickness. Only the results of sample MYC could be fitted to this condition (Fig. 7c). The exponential fits of the results of samples M and MC indicated lower values of transmittance at zero thickness (a and b). These deviations are not predicted by Beer–Lambert–Budworth equation (Eq. (1)).[5]

Budworth's[5] proposed that the coefficient of grain-boundary scattering, S_b, is given by $S_b = x/G$, where x is the factor of grain-boundary scattering and G is the grain size.[5] The factor x can be evaluated by the angular coefficient of the exponential decay of the transmittance with t/G, where t is thickness of the sample.[23] This approach is valid for homogeneous materials, where t/G is the number of grain-boundary intercepts along the cross-section. In the case of materials with BLS grains, the thickness of these grains (~100 μm) affects this number, especially in specimens with 0.5 mm thickness. The average number of grain-boundary intercepts, N, is generically expressed as

$$N = \frac{t - fh}{G} + f \quad (2)$$

where t is the thickness of sample, G is the grain size, h is the thickness of BLS grains, and f is the frequency of occurrence of BLS grains ($f = 2$ for the formation of BLS grains on both sides of the sample).[24] The results of in-line transmittance as a function of number of grain-boundary intercepts, N, are shown in Fig. 8. All three samples presented similar exponential decay of transmittance with the increase of N, and the determined values of grain-boundary scattering factor, x, were ~0.3.

4. Discussion

Burke et al.[16] also observed the formation of entrapped pores in the first 10 μm from the surface inside the BLS grains in alumina doped with 500–1000 ppm MgO sintered in dry hydrogen atmosphere. They argued that the evaporation of MgO from the surface region to a content bellow its solubility limit caused the occurrence of abnormal grain-growth process and formation of BLS grains with initial thickness of ~10 μm. At this stage, the samples were not fully dense and residual pores remained trapped inside the BLS grains. The grains grew laterally with a very rapid rate because of the low MgO content in the sur-

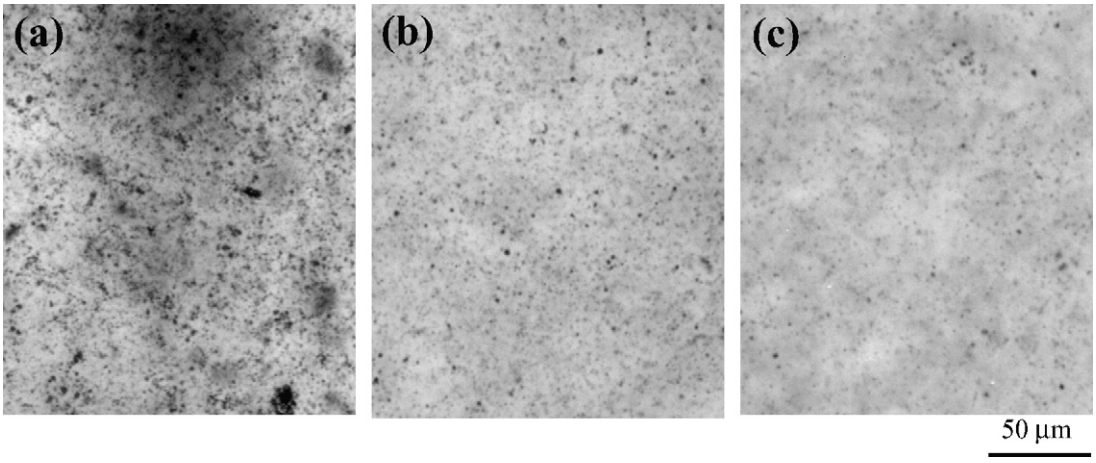

Fig. 4. OM images (transmitted light) showing pores entrapped inside BLS grains in sample M (a); MC (b); MYC (c), sintered for 8 h.

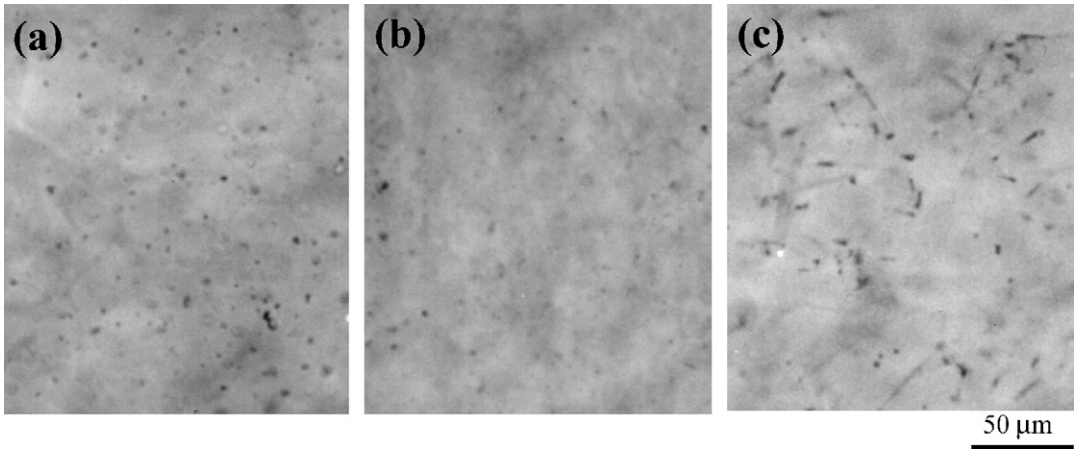

Fig. 5. OM images (transmitted light) showing second-phase particles in internal polycrystalline region of: (a) sample MC sintered for 8 h; (b) sample MYC sintered for 1 h; (c) sample MYC sintered for 8 h.

face region, but the grain-boundary mobility in the direction of thickness was restrained by MgO content above solubility limit at a distance of ~10 μm from the surface. When the remaining volume of sample achieved theoretical density, the BLS grains grew in the thickness direction, leaving a pore free layer inside the BLS grains.[16] This rationale explains the formation of BLS grains (Fig. 1) with a thin layer of entrapped pores near the surface (Fig. 4). Since the fraction of pores entrapped inside BLS grains indicates the densification degree of sample at the moment in which abnormal grain growth occurred,[16] it can be inferred that the addition of CaO and Y_2O_3 in the samples MC and MYC enhanced the densification rate in relation to the sample M. The very low amounts of pores entrapped inside BLS grains in sample MYC (Fig. 4c) indicated that this sample was almost fully dense, when the BLS grains suddenly formed.

The deviations of the values of in-line transmittance at zero thickness observed in samples M and MC (Fig. 7a and b) can be explained if an additional pre-exponential term in Eq. (1) is considered. The scattering phenomenon related to this term should be thickness-invariant. An effect related to the processing of sample, like surface roughness, seems not to explain the deviations of the value of in-line transmittance at zero thickness observed in samples M and MC, since all three samples were prepared following the same processing route. Usually, the scattering caused by residual pores in TPCA is considered thickness-dependent, since they are dispersed homogeneously throughout the section of the material, and their effects in light transmission are included in the scattering coefficient related to the second-phase particles, S_p, an exponential term in Eq. (1). Microstructural analysis, however, showed that the fraction of pores entrapped inside BLS grains is not dependent on the thickness of specimen (Fig. 4). The relative fraction of these pores in samples M and MC (Fig. 4a and b) correlated to the deviations from the expected value of transmittance for zero thickness (Fig. 7a and b). The matching of the results of sample MYC to Beer–Lambert–Budworth model (Fig. 7c) indicated that the pores entrapped inside BLS grains did not affect significantly the light transmission of this sample, in accordance to the results of optical microscopy (Fig. 4c).

Table 1
Results of chemical analysis of the samples before/after sintering (1850 °C, 3 h)

Sample (ppm)	M	MC	MYC
MgO	316/232	297/158	302/58
CaO	6/<5	158/62	54/<5
Y_2O_3	<5/<5	<5/<5	96/95

The effects of residual pores entrapped inside BLS grains can be explained by an introduction of a factor of surface scattering related to the microstructure, S_S, in the Beer–Lambert–Budworth equation (Eq. (1)), as follows:

$$T_I = (1 - R)^2(1 - S_S)^2 \exp[-(\alpha + S_p + S_b)t]. \quad (3)$$

where R, α, S_p, S_b and t have the same meanings as presented for Eq. (1). The fitting of this equation to the experimental results (Fig. 7) made possible the evaluation of factor S_S and in-line loss coefficient ($\alpha + S_p + S_b$) of the samples sintered at different times (Fig. 9). The factor S_S of samples M and MC lowered at slow rates (a), in accordance to the microstructural analysis which showed that fraction of pores entrapped inside BLS grains did not change significantly with the increase of sintering time (Fig. 4). The values of S_S of sample M were around two times those of sample MC. The in-line loss coefficient ($\alpha + S_p + S_b$) of the samples M and MYC decreased strongly with the increase of sintering time and the values of $\alpha + S_p + S_b$ of the sample MYC were around two times those of the sample M (Fig. 9b). Sample MC presented slow decrease of in-line loss coefficient with the increase of sintering time and the values of $\alpha + S_p + S_b$ ranged between the results of samples M and MYC.

Similar to the Budworth's approach,[5] the coefficient of grain-boundary scattering coefficient, S_b, can be calculated by the following relation:

$$S_b = \frac{xN}{t} \quad (4)$$

where x is the factor of grain-boundary scattering, N is the number of grain-boundary intercepts, and t is the thickness of sample. The values of S_b were evaluated for each sintering time (Fig. 10a)

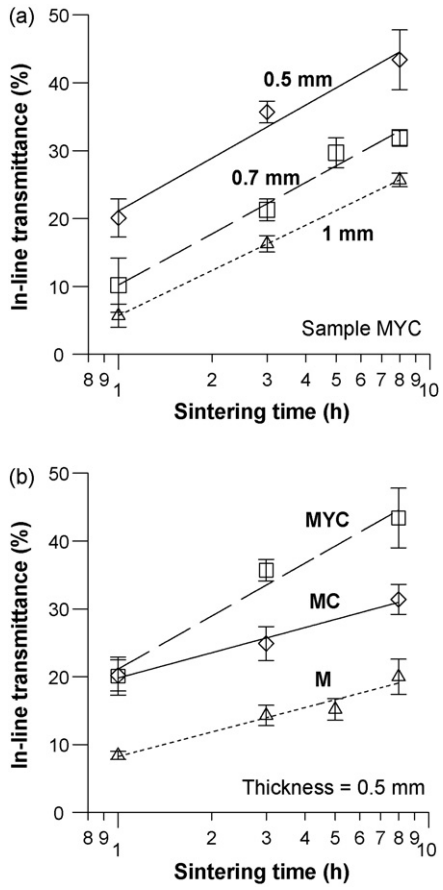

Fig. 6. In-line transmittance at 600 nm as a function of sintering time of: (a) sample MYC with different thickness and (b) samples M, MC and MYC with 0.5 mm thickness.

using the determined value of factor of grain-boundary scattering, x (Fig. 8). The values of S_b of the three samples lowered significantly and similarly with the increase of sintering time, but the scaling value varied among the samples (Fig. 10a). Sample MC presented lower values of S_b than sample M, mainly because of larger grain size and thickness of BLS grains (Fig. 3). Sample MYC, however, presented slightly higher values of S_b than sample M, despite its larger grain size and thickness of BLS grains (Fig. 3). It has been suggested that additives or impurities segregated to grain-boundaries can affect the light transmission in TPCA.[28,29] In fact, it has been observed that yttrium segregates to grain-boundaries and pore surfaces in an ultra-high-purity alumina doped with Y_2O_3.[30] Therefore, the results suggest that the segregation of Y_2O_3 additive altered the optical properties of alumina grain-boundaries, increasing the light scattering.

The scattering coefficient of second-phase particles, S_p, was evaluated from the difference of the results of in-line transmittance loss coefficient, $\alpha + S_p + S_b$ (Fig. 8b), and grain-boundary scattering coefficient, S_b (Fig. 10a), since the intrinsic absorption coefficient, α, of single-crystal alumina is low ($0.01\ cm^{-1}$) and negligible compared to the others scattering coefficients.[6] From Mie scattering theory, the light scattering achieves a maximum when the particle size is around the same value of the wavelength of visible light.[3,4] The S_p values of sample MYC decreased rapidly with the increase of sintering time (Fig. 10b), which seems to be related to the coarsening of second-phase particles (Fig. 5b and c). The S_p values of sample MC increased slightly with the increase of sintering time (Fig. 10b). The slight increase of second-phase particle size observed by microstructural analysis indicated that coarsening in this case adjusted the particle size distribution toward the maximum scattering. The smaller particle size observed in sample MC compared to sample MYC (Fig. 5a and c) supports this rationale. The evaluated

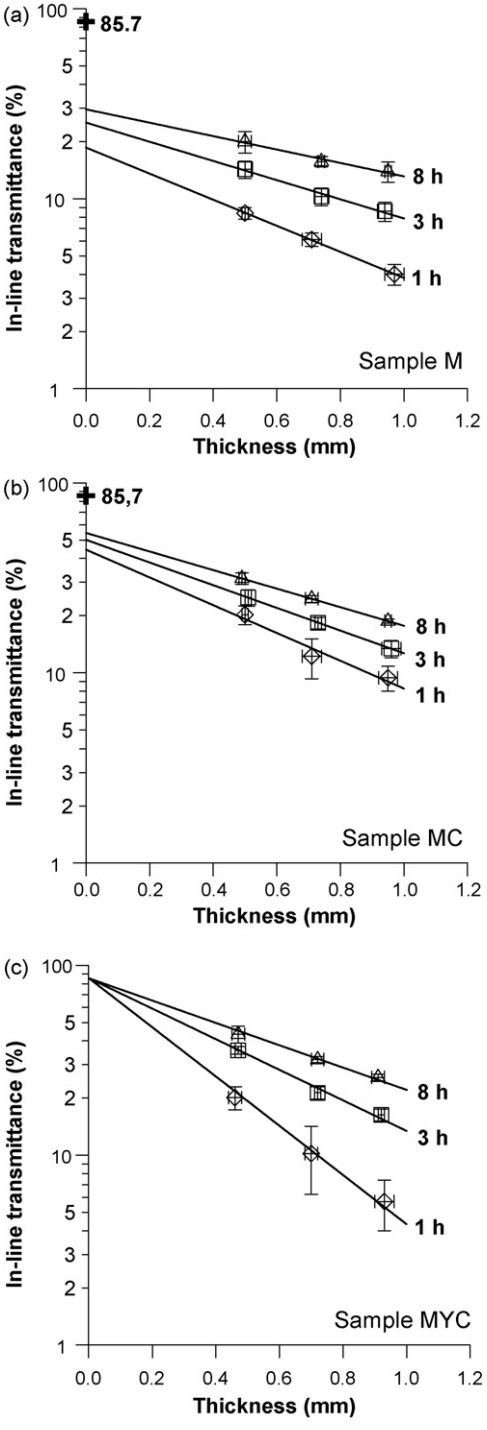

Fig. 7. In-line transmittance as a function of specimen thickness of: (a) sample M; (b) sample MC; (c) sample MYC.

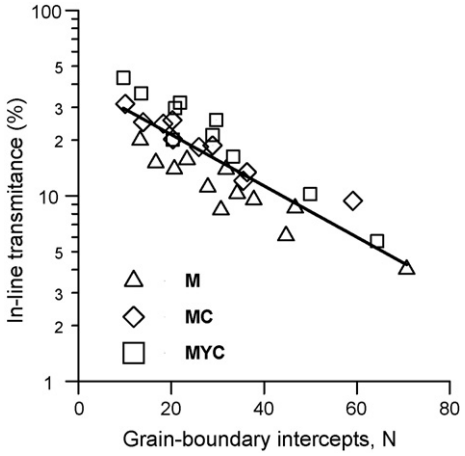

Fig. 8. In-line transmittance, T_I, as a function of number of grain-boundary intercepts, N.

S_p values of sample M were very close to zero for all sintering times, in accordance to the microstructure analysis, indicating that the internal polycrystalline region of this sample was almost devoid of second-phase particles.

Using the scattering coefficients evaluated (Figs. 9 and 10), the effects of each scattering center in the reduction of direct

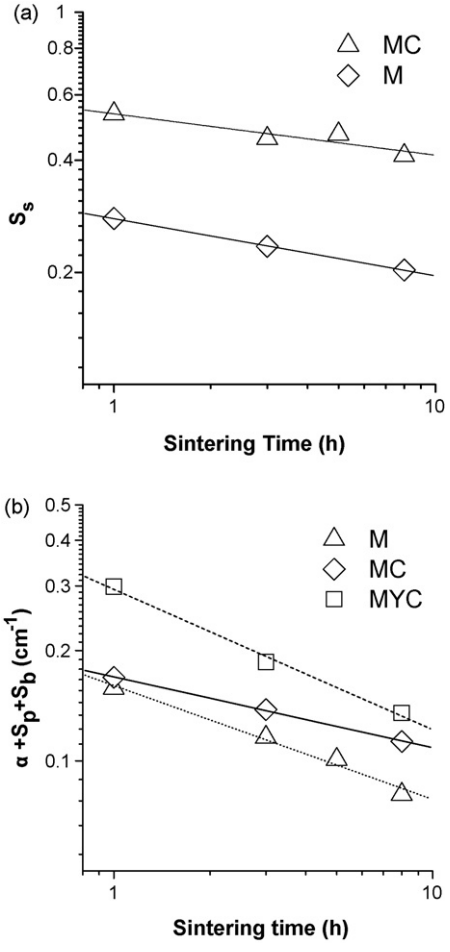

Fig. 9. Factor of surface scattering related to the microstructure, S_S (a), and in-line loss coefficient, $\alpha + S_p + S_b$ (b), as a function of sintering time.

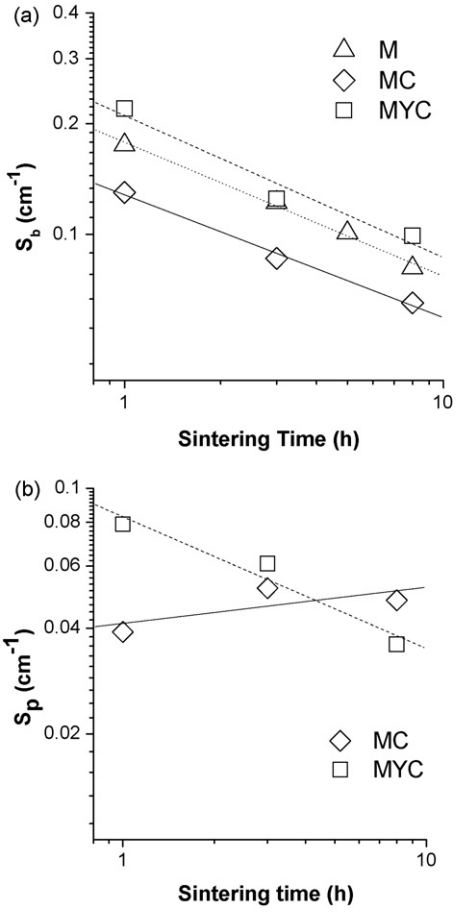

Fig. 10. Scattering coefficient of grain-boundary, S_b (a), and of second-phase particles, S_p (b), as a function of sintering time.

light transmission were estimated (Fig. 11). For sample M, the reduction of in-line transmittance, T_I, was caused mainly by the residual pores entrapped inside BLS grains (field S_S in Fig. 11a), and the rate of decrease of T_I with thickness was defined by grain-boundary scattering (field S_b in a). For sample MC, this rate was defined by both scattering centers: grain-boundaries and second-phase particles (fields S_b and S_p in b), with slightly larger influence of scattering by grain-boundaries. For sample MYC, the reduction of in-line transmittance, T_I, with thickness was defined mostly by grain-boundary scattering (field S_b in c), with smaller effect of scattering by second-phase particles (field S_p in c).

The effects of scattering by optical heterogeneities that determined the positive logarithmic dependence of in-line transmittance with sintering time (Fig. 6) were also evaluated (Fig. 12). For sample M, the slow increase of in-line transmittance, T_I, with sintering time was controlled by the slow rate of pore elimination in BLS grains (Fig. 4a), since the lowering of grain-boundary scattering caused by grain growth (Fig. 10a) was small compared to the scattering by pores entrapped inside BLS grains (Fig. 12a). For sample MC, the slow increase of T_I with sintering time was also controlled by the slow rate of pore elimination in BLS grains, since the lowering of grain-boundary scattering caused by grain growth was mostly counterbalanced by the increase of scattering by second-

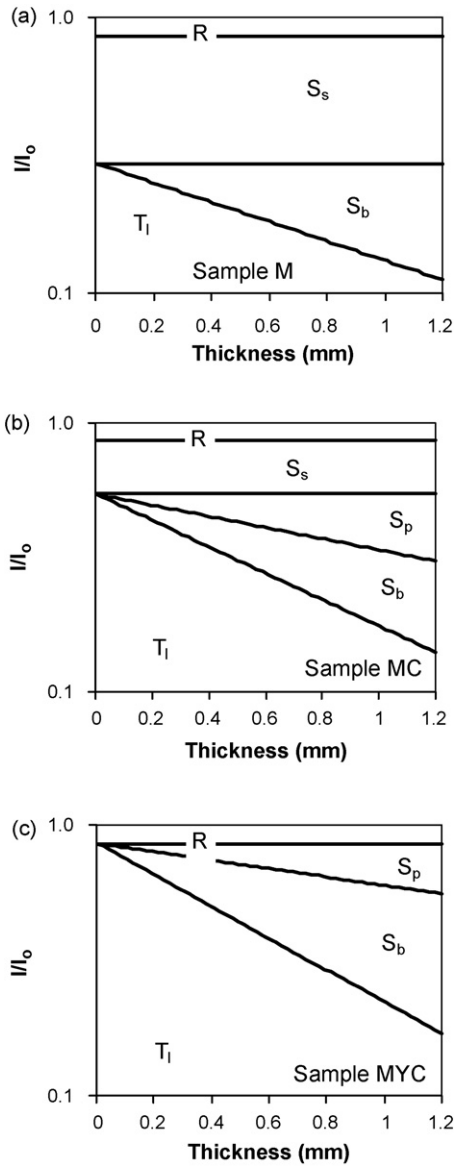

Fig. 11. Optical properties—thickness diagrams of the samples sintered for 8 h. The field indicated with letter T_I is direct light transmission, R is transmission loss by surface reflection, S_S is transmission loss by light scattering centers related to the surface (pores entrapped inside BLS grains), S_b is transmission loss by grain-boundary scattering, and S_p is transmission loss by second-phase particles. The ratio I/I_0 represents the fraction of transmitted or scattered light intensity in relation to the intensity of incident light beam.

phase particles (Fig. 12b). The scattering by pores entrapped inside BLS grains had the most significant influence on loss of light transmission of sample MC, followed by scattering by grain-boundaries and scattering by second-phase particles (b). For sample MYC, the rapid increase of T_I with sintering time was caused by the rapid decrease of both scatterings: grain-boundaries and second-phase particles (c).

The main factor that defined the differences of in-line transmittance, T_I, among the samples was the scattering by residual pores entrapped inside BLS grains. Sample MC presented higher values of T_I than sample M mainly because of lower fraction of these pores, which resulted in lower factor of surface scattering related to the microstructure, S_S (Fig. 8a). The effect of scattering by grain-boundaries was stronger in sample MYC than in samples M and MC, but the negligible scattering by pores entrapped inside BLS grains resulted in the highest values of in-line transmittance. Therefore, the main benefic effect of addition of CaO and Y_2O_3 to the increase of in-line transmittance was the lowering of fraction of pores entrapped inside BLS grains (Fig. 4). The addition of these oxides enhanced the densification rate in the last stage of sintering and resulted in a denser alumina body when the BLS grains formed. The addition of CaO and Y_2O_3, however, had other effects: (i) the addition of CaO lowered the coefficient of grain-boundary scattering, S_b, of the sample MC and the addition of Y_2O_3 increased the S_b values of the sample MYC, in relation to the sample M (Fig. 10a) and (ii) the addition of CaO and Y_2O_3 affected negatively the light transmission by enhancing the coefficients of second-phase particle scattering, S_p, of the samples MC and MYC, in relation to the sample M (Fig. 10b).

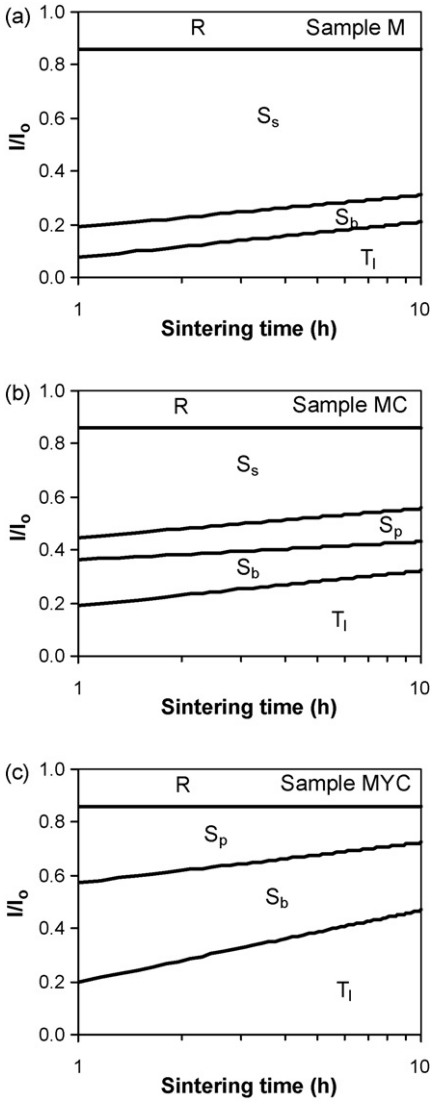

Fig. 12. Optical properties—sintering time diagrams (samples with 0.5 mm thickness). The fields T_I, R, S_S, S_b, S_p and ratio I/I_0 have the same meanings as presented in Fig. 11.

An important characteristic of TPCA for discharge lamps is corrosion resistance against the aggressive hot atmosphere in discharge envelopes. In high-pressure sodium (HPS) lamps, corrosive sodium plasma arc limits lamp performance, since sodium reacts with Al_2O_3 to form sodium aluminate (β-Al_2O_3) and metallic aluminum during lamp operation. It has been shown that the grain-boundaries are rapid pathways for diffusion of reactant (sodium) and reaction products (aluminum).[14] Some impurities or additives, like CaO and MgO, segregated at grain-boundaries decrease the resistance against sodium corrosion.[31] Second-phase particles, usually located at alumina grain-boundaries, can also affect corrosion rate. Spinel particles seem to promote the formation of β-Al_2O_3 and accelerate sodium attack, while YAG particles are resistant to this attack.[14] Since grain-boundaries usually enhance the corrosion rate in TPCA, it is expected that the elimination of grain-boundaries near the surface, by the formation of BLS grains, can significantly increases the corrosion resistance against the aggressive atmospheres. A corrosion study, however, is necessary in order to confirm the hypothesis that the alumina ceramics with bi-dimensionally large surface grains have an increased corrosive stability compared with more fine-grained surface microstructures.

5. Conclusions

Alumina ceramics with bi-dimensionally large surface (BLS) grains and high in-line transmittance (up to ~40% at 0.5 mm-thickness) were prepared. These grains were flat, parallel to the surface with ~100 μm-thickness and lateral sizes up to the millimeter range. The key factor that limited the light transmission in these materials was the formation of a thin layer of pores entrapped inside the large surface grains within a narrow zone at 10–20 μm distance from the surface. The fraction of these pores is thickness-invariant. The introduction of a surface scattering factor related to the microstructure, S_S (Eq. (3)), made possible the quantification of the effects of different scattering centers. The addition of CaO and Y_2O_3, together with MgO, lowered significantly the factor S_S (that is, lowered the fraction of pores entrapped inside the BLS grains) and also affected the scattering coefficients of grain-boundaries, S_b, and second-phase particles, S_p. The in-line transmittance of samples M (300 ppm MgO) and MC (300 ppm MgO and 150 ppm CaO) increased slowly with the increase of sintering time, because of the slow rates of pore elimination in BLS grains. The rapid increase of in-line transmittance of sample MYC (300 ppm MgO, 100 ppm Y_2O_3 and 50 ppm CaO) was caused by the rapid decrease of coefficients S_b and S_p with the increase of sintering time.

Acknowledgements

The authors acknowledge the Japanese agency JICA and Brazilian agencies FAPESP and CNPq for the financial support of the present research.

References

1. Coble, R. L., Transparent alumina and method of preparation. U.S. Patent No. 3,026,210, 1962.
2. Wei, G. C. and Rhodes, W. H., Sintering of translucent alumina in a nitrogen–hydrogen gas atmosphere. *J. Am. Ceram. Soc.*, 2000, **83**(7), 1641–1648.
3. Peelen, J. G. J. and Metselaar, R., Light scattering by pores in polycrystalline materials: transmission properties of alumina. *J. Appl. Phys.*, 1974, **45**(1), 216–220.
4. Apetz, R. and Van Bruggen, M. P. B., Transparent alumina: a light-scattering model. *J. Am. Ceram. Soc.*, 2003, **86**(3), 480–486.
5. Budworth, D. W., Transparency of polycrystalline ceramics. In *Special Ceramics 5*, ed. P. Popper. The British Ceramic Research Association, 1972, pp. 185–192.
6. Yoshimura, H. N., Camargo, A. C., Goulart, E. P. and Maekawa, K., Translucent polycrystalline alumina: influence of roughness and thickness on in-line transmittance. *Mater. Sci. Forum*, 1999, **299–300**, 35–40.
7. Grimm, N., Scott, G. E. and Sibold, J. D., Infrared transmission properties of high density alumina. *Ceram. Bull.*, 1971, **50**(12), 962–965.
8. Rhodes, W. H., Sellers, D. J. and Vasilos, T., Hot-working of aluminum oxide. II. Optical properties. *J. Am. Ceram. Soc.*, 1975, **58**(1–2), 31–34.
9. Toda, G., Noro, T. and Muta, A., Effects of Y_2O_3 and MgO addition on transmittance of sintered Al_2O_3. *Fummatsu Oyobi Fummatsu-Yakin*, 1974, **21**(3), 12–17.
10. Oda, I. and Maekawa, K., Method for producing polycrystalline translucent alumina having an excellent in-line transmission. U.S. Patent No. 4,222,978, 1980.
11. Kaneno, M. and Kajihara, T., Polycrystalline translucent alumina sintered body, a method for producing the same and a high pressure vapor discharge lamp obtained by using said sintered body. U.S. Patent No. 4,495,116, 1985.
12. Charles, R. J., Prochazka, S. and Scott, C. E., Alumina ceramic. U.S. Patent No. 4,285,732, 1981.
13. Takahashi, H., Umezaki, H. and Teshima, Y., Translucent polycrystalline alumina and process for producing the same. U.S. Patent No. 5,382,556, 1995.
14. Wei, G. C., Hecker, A. and Goodman, D. A., Translucent polycrystalline alumina with improved resistance to sodium attack. *J. Am. Ceram. Soc.*, 2001, **84**(12), 2853–2862.
15. Greskovich, C. and Brewer, J. A., Solubility of magnesia in polycrystalline alumina at high temperatures. *J. Am. Ceram. Soc.*, 2001, **84**(2), 420–425.
16. Burke, J. E., Lay, K. W. and Prochazka, S., The effect of MgO on the mobility of grain boundaries and pores in aluminum oxides. *Sintering Processes*. Plenum Press, New York, 1980, pp. 417–425.
17. Scott, C., Kaliszewski, M., Greskovich, C. and Levinson, L., Conversion of polycrystalline Al_2O_3 into single-crystal sapphire by abnormal grain growth. *J. Am. Ceram. Soc.*, 2002, **85**(5), 1275–1280.
18. Wei, G. C., Transparent ceramic lamp envelope materials. *J. Phys. D: Appl. Phys.*, 2005, **38**, 3057–3065.
19. Thompson, G. S., Henderson, P. A., Harmer, M. P., Wei, G. C. and Rhodes, W. H., Conversion of polycrystalline alumina to single-crystal sapphire by localized codoping with silica. *J. Am. Ceram. Soc.*, 2004, **87**(10), 1879–1882.
20. Krell, A., Blank, P., Ma, H., Hutzler, T., Van Bruggen, M. P. B. and Apetz, R., Transparent sintered corundum with high hardness and strength. *J. Am. Ceram. Soc.*, 2003, **86**(1), 12–18.
21. Krell, A. and Klimke, J., Effects of the homogeneity of particle coordination on solid-state sintering of transparent alumina. *J. Am. Ceram. Soc.*, 2006, **89**(6), 1985–1992.
22. Yoshimura, H. N., Da Cruz, A. C. and Goldenstein, H., Characterization of sub-superficial defects in translucent alumina using a liquid immersion technique in transmitted light microscopy. *Improved Ceramics through New Measurements, Processing, and Standards*. The American Ceramic Society, 2002, pp. 145-150.
23. Smethurst, E. and Budworth, D. W., The preparation of transparent magnesia bodies. I. By hot-pressing. *Trans. J. Br. Ceram. Soc.*, 1972, **71**(2), 45–50.

24. Yoshimura, H. N., Translucent alumina with addition of MgO, CaO and Y_2O_3. Ph.D. Thesis, Polytechnic School of the University of São Paulo, Brazil, 2000.
25. Bennison, S. J. and Harmer, M. P., Grain-growth kinetics for alumina in the absence of a liquid phase. *J. Am. Ceram. Soc.*, 1985, **68**(1), C22–C24.
26. Rhodes, W. H., Polycrystalline oxides for optical applications. In *Ceramics: Today and Tomorrow*, ed. S. Naka *et al.* The Ceramic Society of Japan, Tokyo, 1986, pp. 149–164.
27. Levin, E. M., Robbins, C. R. and McMurdie, H. F., *Phase Diagrams for Ceramists*, *vol. 2*, ed. M. K. Reser. The American Ceramic Society, Ohio, 1969, p. 129.
28. Yamamoto, N., Translucent polycrystalline alumina ceramics. In *Proceedings of the Symposium on Research and Development Trend on Optoceramics*, 1984, pp. 22–30.
29. Kwon, O.-H., Nordahl, C. S. and Messing, G. L., Submicrometer transparent alumina by sinter forging seeded γ-Al_2O_3 powders. *J. Am. Ceram. Soc.*, 1995, **78**(2), 491–494.
30. Thompson, A. M., Soni, K. K., Chan, H. M., Harmer, M. P., Williams, D. B., Chabala, J. M. and Levi-Setti, R., Dopant distributions in rare-earth-doped alumina. *J. Am. Ceram. Soc.*, 1997, **80**(2), 373–376.
31. De With, G., Vrugt, P. J. and Van de Ven, A. J. C., Sodium corrosion resistance of translucent alumina: effect of additives and sintering conditions. *J. Mater. Sci.*, 1985, **20**, 1215–1221.